

ARTICLE OPEN

Two-dimensional iodine-monofluoride epitaxy on WSe₂Yung-Chang Lin¹, Sungwoo Lee², Yueh-Chiang Yang³, Po-Wen Chiu³ and Gun-Do Lee² and Kazu Suenaga¹

Interhalogen compounds (IHCs) are extremely reactive molecules used for halogenation, catalyst, selective etchant, and surface modification. Most of the IHCs are unstable at room temperature especially for the iodine-monofluoride (IF) whose structure is still unknown. Here we demonstrate an unambiguous observation of two-dimensional (2D) IF bilayer grown on the surface of WSe₂ by using scanning transmission electron microscopy and electron energy loss spectroscopy. The bilayer IF shows a clear hexagonal lattice and robust epitaxial relationship with the WSe₂ substrate. Despite the IF is known to sublime at -14 °C and has never found as a solid form in the ambient condition, but surprisingly it is found stabilized on a suitable substrate and the stabilized structure is supported by a density functional theory. This 2D form of IHC is actually a byproduct during a chemical vapor deposition growth of WSe₂ in the presence of alkali metal halides as a growth promoter and requires immediate surface passivation to sustain. This work points out a great possibility to produce 2D structures that are unexpected to be crystallized or cannot be obtained by a simple exfoliation but can be grown only on a certain substrate.

npj 2D Materials and Applications (2021)5:18; <https://doi.org/10.1038/s41699-021-00201-8>

INTRODUCTION

Since one atomic layer of carbon was isolated from the bulk graphite by exfoliation as graphene¹, other elements and chemical compounds, such as silicon², germanium³, boron⁴, phosphorus⁵, hexagonal boron nitride (hBN)⁶, and transition metal dichalcogenides (TMDCs)⁷, have been extensively tested to form atomically thin planar structures over the past decade. Choosing a suitable substrate is the key to realize monolayer epitaxy out of the natural layered crystals, and is also essential to lower the formation energy of those elements to form 2D structures on the surface instead of forming 3D bulk solids^{8,9}.

Halogens also have been predicted to form 2D structures with compressed or expanded forms when absorbed on solid surfaces in the 1980s¹⁰. Halogen adsorption is of technological importance in many fields, such as anisotropic dry etching, the catalyst for chemical reaction, oxychlorination reaction, and electrochemistry for battery operation. Iodine is the largest atom of halogens, except for astatine, and has the lowest electronegativity and largest polarizability, which makes iodine more flexible in coordinate bonding. In the 1980s, the atomic iodine layer chemisorbed on Pt single-crystal surface was studied in an ultra-high vacuum chamber with low energy electron diffraction and Auger electron spectroscopy^{11,12}.

In the chemical vapor transport method, halogens (I₂ or Br₂) and halogenides are essential to transport agents to grow layered TMDCs under equilibrium condition¹³. The solid TMs sources can be transformed into a gaseous metal halide with the presence of halogens which can effectively lower the growth temperature during vapor transport growth. Recently, alkali metal halides (i.e., KI and NaCl) were also used as the growth promoters to synthesize numerous types of monolayer TMDCs through chemical vapor deposition^{7,14}. Some early studies discussed the possibility of intrinsic doping of TMDCs with the halogen incorporation from the transport agents^{13,15} which suggests that the TMDCs might have been functionalized by the coverage of 2D halogens on the surface. Since the halogens possess strong electronegativity, the

formation of 2D halogen compounds would be potentially an effective way for surface modification on the layered materials. However, up to date, the reports related to the 2D halogen compounds are few and the actual structures have not been directly assigned yet. Here in this letter, we report a direct visualization of 2D interhalogen compound, iodine monofluoride (IF), grown on the surface of WSe₂ by using scanning transmission electron microscopy (STEM). The 2D IF layer was formed as a bilayer and arranged in hexagonal symmetry which was supported by a density functional theory (DFT) study. Atomic probe electron energy loss spectroscopy (EELS) was utilized for identifying the chemical composition of iodine monofluoride. This is the observation of crystalline 2D IHC which is beyond the knowledge of material science. Our findings can break through the perception and theory of the fundamental metallurgy.

RESULTS AND DISCUSSION

Synthesis and characterization of 2D iodine-monofluoride on WSe₂

During a chemical vapor deposition method to grow WSe₂, we added potassium iodide (KI) and Sodium fluoride (NaF) as the growth promoter. The experimental setup is shown in Fig. 1 and the growth detail is presented in the method. The grown WSe₂ with the possible halogenated surface was passivated with a layer of polycarbonate immediately after the growth and gently transferred to TEM Cu quantify oil by using the well-established clean transfer technique^{16,17}.

Figure 2a shows a wide area annular dark field (ADF) image of the WSe₂ with extra platelet structures covering the surface. Almost 50% of the WSe₂ substrate (dark contrast) is covered by the extra surface layer in brighter contrast. An EELS chemical analysis (Fig. 2b) shows the brighter contrast layer is a compound of iodine and fluorine. The W and Se peaks are shown in the low energy region around 40–50 eV. The red spectrum shows a clear iodine signal at 650 eV and fluorine edge at ~700 eV. At low

¹Nanomaterials Research Institute, National Institute of Advanced Industrial Science and Technology (AIST), Tsukuba 305-8565, Japan. ²Department of Materials Science and Engineering and Research Institute of Advanced Materials, Seoul National University, Seoul, Republic of Korea. ³Department of Electrical Engineering, National Tsing Hua University, Hsinchu 30013, Taiwan. ✉email: yc-lin@aist.go.jp; pwchiu@ee.nthu.edu.tw; gdllee@snu.ac.kr

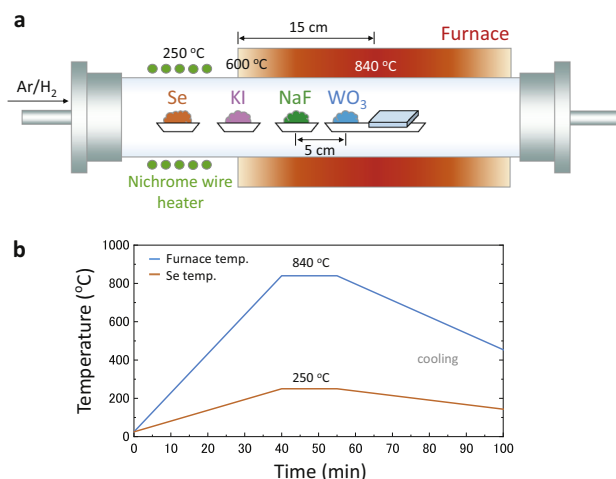


Fig. 1 CVD growth of 2D IF layer on WSe₂. **a** Schematic of the WSe₂ growth with adding KI and NaF as the growth promoter. **b** Temperature–time plot of the WSe₂ growth.

energy region, iodine edge at 50 eV is overlapping with W and Se peaks which gives extra background to the WSe₂ substrate spectrum. A quantitative analysis shows a wide range of the atomic ratio $0 < F:I < 4$ (Supplementary Fig. 1), which suggests strong beam damage happening during the EELS experiments resulting in severe changes in the composition from the stoichiometric value. In fact, a few seconds of acquisition time for EELS always destroys the IF layers, and no longer time acquisition with a better statistic is possible. Halogens are actually known for their beam sensitivities. The IF layer was originally a continuous film with a size of about $0.07 \mu\text{m}^2$ as pointed by the white arrows in a low-magnification image of Fig. 2a inset. The ADF contrast of the IF layer is slightly weaker than the overgrown WSe₂ bilayer pointed by the black arrow and is distinguishable from the second layer of WSe₂. In order to minimize the electron beam damage in observation at high magnification, we moved the specimen under the gun valve closed condition prior to the image acquisition. A moiré pattern is formed at IF and WSe₂ overlapping area which is more clearly seen in the magnified ADF image shown in Fig. 2c. The fast Fourier transform (FFT) image shown in Fig. 2d displays the structure information of the 2D IF/

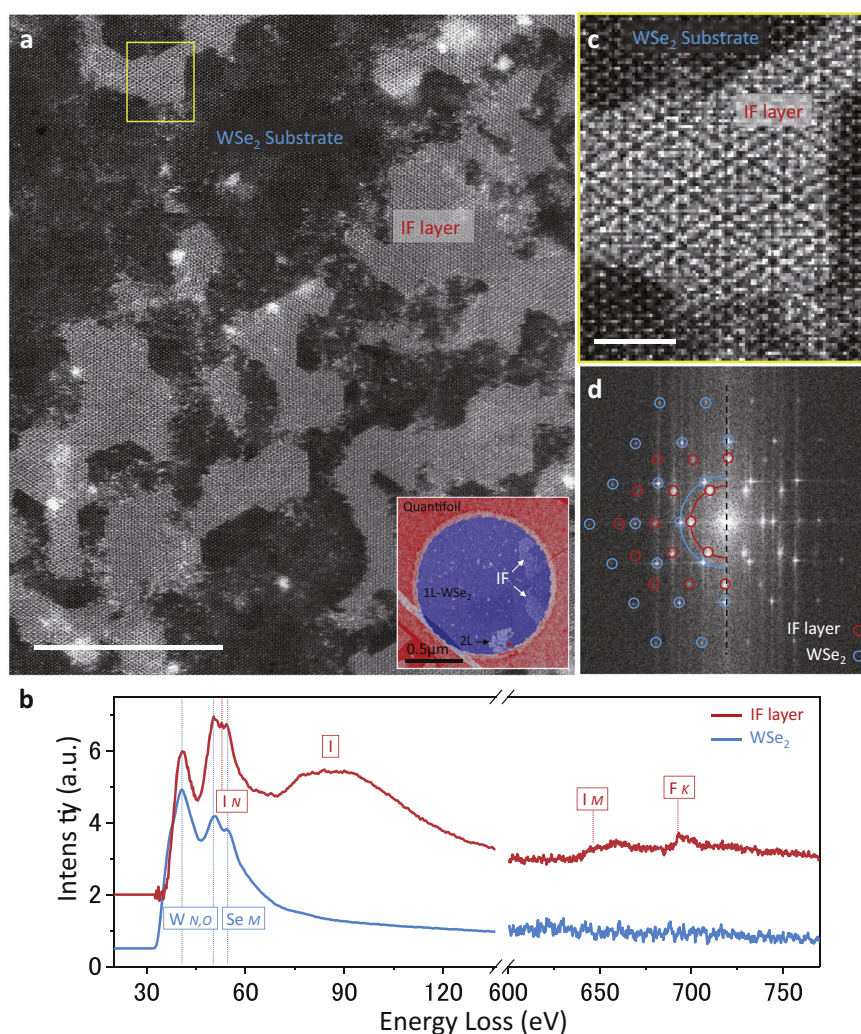


Fig. 2 STEM and EELS characterization of 2D IF layer. **a** A STEM-ADF image of IF layer is grown on WSe₂ substrate. The scale bar is 20 nm. **b** EEL spectra of the IF layer (red spectrum) and WSe₂ substrate (blue spectrum) taken from the brighter layer and the dark region in (a), respectively. **c** A closeup of the yellow rectangle area in (a), which shows a moiré pattern of the surface IF layer with the WSe₂ substrate. The scale bar is 2 nm. **d** An FFT pattern of the whole image in (a), where the left part marked with red and blue circles in the diffraction spots showing a clear epitaxial relationship of the surface IF layer and the WSe₂ substrate.

WSe₂ which shows a clear epitaxial relationship of the surface IF layer and the WSe₂ substrate. One can see the two sets of hexagonal diffraction patterns refer to the structure of WSe₂ (blue circles) and the IF layer (red circles) shown in Fig. 2d. The structure of the 2D IF layer appears hexagonal symmetry in the crystal *c*-axis. Note that the IF layer survives only the first scan and will go away instantly in the second. The IF layers are also sensitive to laser excitation, which makes it difficult for us to obtain their optical spectra.

Structural analysis of the 2D iodine-monofluoride

Most of the ever-recognized interhalogen compounds are known as molecules consisting of two different halogen atoms (i.e., fluorine, chlorine, bromine, and iodine) without elements from other groups. The gas-phase IF was firstly identified by its emission spectrum (435–690 nm) in 1951¹⁸ and its laser response was also reported^{19,20}. The interhalogen compounds are assembled in the forms of XY_{*n*} (*n* = 1, 3, 5 or 7, X is the heavier or less electronegative halogen, Y is the lighter or more electronegative halogen) by halogen atoms reaction at high temperature. They are very reactive and have covalent bonds in nature with diamagnetic due to the existence of bond pairs and lone pairs. Most of the X–Y bond in interhalogens is much weaker than the X–X bond in halogens, except for the F–F bond because F has the strongest electronegativity with the possible ionic charge of only –1. The IF is a powder below –58 °C and sublimates at –14 °C which cannot be isolated as a pure substance and should disproportionate rapidly into elemental iodine and iodine trifluoride at room temperature²¹.

The IF layer existing on WSe₂ surface at room temperature is, therefore, extremely surprising. The IF layer alone is not stable in air but probably stable in air for a short time when it absorbs to the WSe₂ surface. We transferred specimens in a vacuum-sealed package and minimized the exposure time before the STEM observations. Figure 3a shows the raw ADF image of the IF/WSe₂ layer with a clear moiré pattern. In order to visualize the structure of the IF layer, we applied an image filtering to the FFT pattern by masking the WSe₂ spots (Fig. 3b), and the inversed FFT image presenting only the IF structure is shown in Fig. 3c. The 2D IF layer clearly exhibits in hexagonal structure with homogeneous contrast. Recently IF compounds have been predicted to crystallize in the 2D planner structure at high-pressure condition^{22,23}. Numerous possible 2D atomic configurations of IF_{*n*} (*n* = 1, 3, 5, or 7) were searched globally using an evolutionary algorithm combined with DFT calculations but the IF structure was the only one found to match our experiments. The IF molecule was found relatively stable as a linear chain structure than the other formation but still cannot preserve the structure as a monolayer IF chain array. The most stable 2D IF structure is bilayer IF chain array stacking with 120° rotation as shown in Supplementary Fig. 2. The formation energy of the IF bilayer is –4.76 eV per unit IF, while it is –4.89 eV when IF epitaxy on WSe₂. Figure 3e shows the atomic model of the IF layer on the WSe₂ surface. The calculated unit cell constant of the IF bilayer is 4.297 Å which is 1.3 times larger than the WSe₂ lattice (3.289 Å). The simulation image based on this theoretical atomic model is shown in Fig. 3d, which matches extremely well with the experimental image shown in Fig. 3a. The IF bilayer was also found 30° rotational stacking on the WSe₂ surface, which suggests an again a strong epitaxial relationship with the substrate. The ADF image in Fig. 3f shows the epitaxial IF layer on the WSe₂ surface consisting of 0° and 30° rotational domains highlighted by cyan and yellow lines, respectively. The IF structural orientation can be clearly seen in the FFT image in the inset and also the inversed FFT image (Fig. 3g) after the WSe₂ structure been filtered out. The simulation image of 30° epitaxial IF layer on WSe₂ shown in Fig. 3h again fits greatly well with the experimental image. According to our DFT

calculation, the IF layer is energetically stable on the surface of 2D materials. So, it should be possible to epitaxy 2D IHCs on the surface of graphene or hBN. The reproducibility of the epitaxy IF layer on 2D materials should be high once the iodine and fluoride sources are added to the synthesis system, however, the stability of the IF layer is extremely low in the ambient condition. The preserving of the IF layer is still challenging, but we believe it can be stabilized under an inert environment.

Theoretical electronic properties of the 2D iodine-monofluoride

This is the direct proof of any interhalogen compound in a 2D crystal structure form. Figure 4a shows a colored ADF of the IF bilayer image after filtering out the WSe₂ contrast. The STEM simulation image and the corresponding atomic model of the IF bilayer are shown in Fig. 4b, c. As we have known the ADF contrast is proportional to the atomic mass where heavier atom gives rise to brighter ADF contrast. As a result, the contrast of fluorine (*Z* = 9) is much weaker than the iodine (*Z* = 53) and is barely seen in both the experimental and the simulation images. The hexagonal atomic configuration is basically contributed by the contrast of iodine atoms. The IF is a parallelly assembled linear chain structure with a distance of 3.8 Å. The second layer of IF is stacking with an in-plane rotation of 120°. The iodine atoms in the bilayer IF form a hexagonal arrangement in the top view. Figure 4d displays the energy band profile of the IF bilayer along with high-symmetry points. The IF bilayer is calculated as a semiconductor with an indirect energy gap of ~0.19 eV if free-standing. The WSe₂ is a semiconductor with a direct energy gap of ~1.64 eV (Fig. 4e), while the band structure becomes metallic when IF bilayer absorbed on WSe₂ as shown in Fig. 4f. The transition from semiconductor to metal is caused by the interaction between IF bilayer and WSe₂ as shown in the density of states and charge density difference analysis as shown in Fig. 4g, h. The main factor of semiconductor to metal transition is the Fermi level shift as electrons in the Se *p*-orbital transferred to I *p*-orbital. The IF epitaxial adhesion can be a robust surface modification material to improve the contact with metal electrodes in electronic devices.

The IF should possess a physical property intermediate between iodine and fluorine. Our report on the epitaxial growth of IF opens up another bottom-up process to assemble unstable elements in a 2D form on the surface of 2D materials. A suitable passivation layer is necessary to preserve the 2D IF layer for further applications. This can be particularly useful for gas detection, ohmic contact engineering, conductivity, and magnetic property modulation especially beneficial in the design of van der Waals heterostructures. Our findings unveil the understanding of halogen surface absorption which is helpful for the modeling of the surface halogenation process and we expect to inspire more research interests in surface physics and material science.

METHODS

Material growth

The WSe₂ was grown in a 1-in. quartz tube placed in a single-zone tube furnace. We used WO₃ (300 mg) as the metal precursor and placed it at the center of the furnace. The growth substrate, sapphire, was placed in close proximity to the WO₃ source at the downstream side. The Se (500 mg) source was placed the upstream of gas flow and heated using an independent nichrome wire heater. Alkali metal halides (KI and NaF) were added as the growth promotor. KI (0.85 mg) was placed at the edge of the tube furnace, which is 15 cm from the furnace center, while the NaF was placed 5 cm in front of the WO₃. The growth process was controlled at low pressure (15 Torr) with the flow of Ar (120 sccm) and H₂ (30 sccm). The quartz tube was purged with Ar and pumped to a base pressure of 0.1 Torr at 100 °C for 30 min prior to the growth. Then the furnace center was heated to 840 °C in 40 min with maintaining the pressure of 15 Torr. During the growth, the Se was heated to 250 °C and the temperature of KI at the

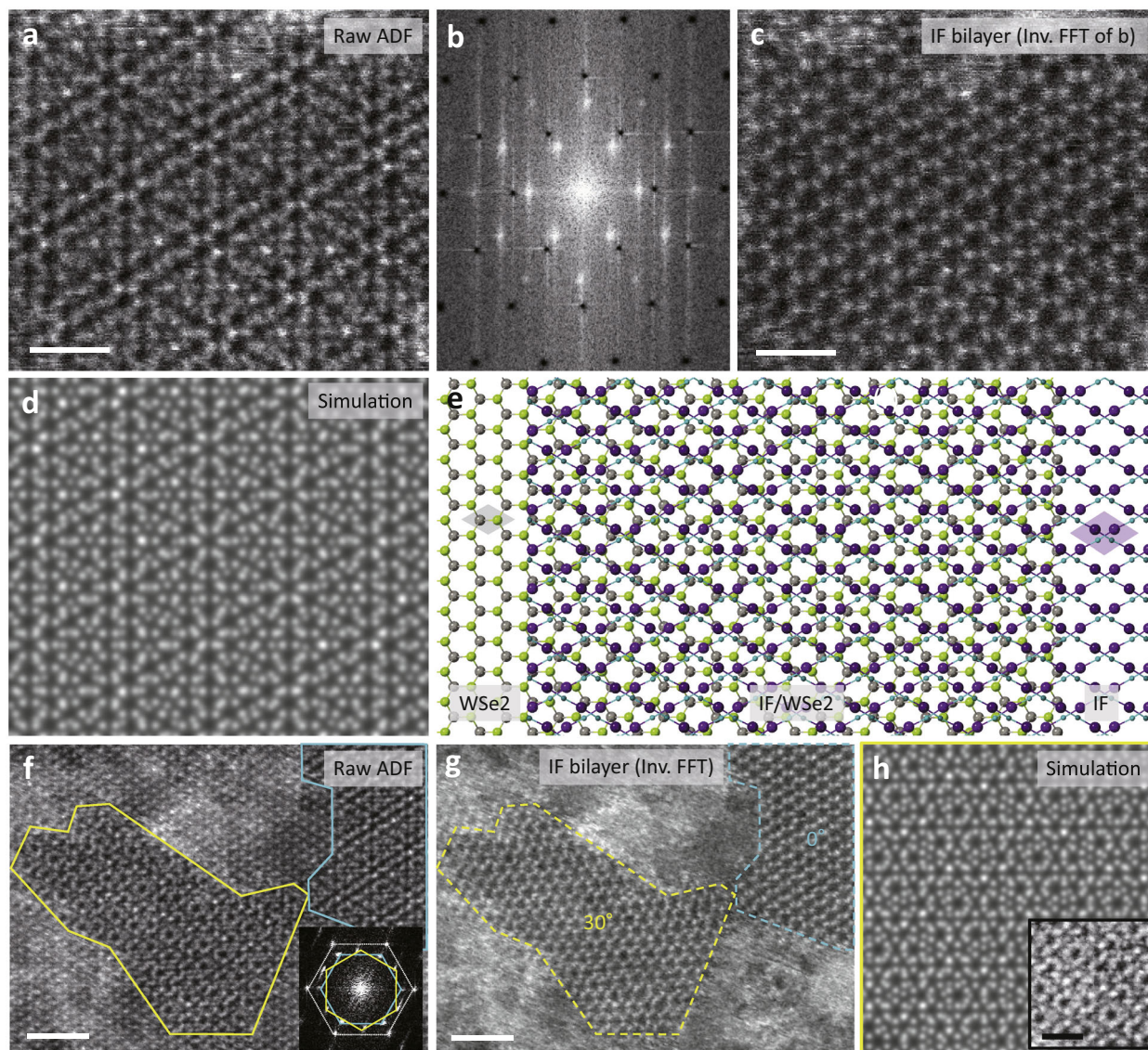


Fig. 3 Structure and stacking order of 2D IF layer on WSe_2 . **a** The intact ADF image of the IF layer on the WSe_2 substrate. The scale bar is 1 nm. **b** The masked FFT pattern of **a** used for the image filtering. **c** An inverted FFT filtered image of the IF layer after the contrast from the WSe_2 substrate been removed. The scale bar is 1 nm. **d** A simulated STEM-ADF image of the atomic models of the IF layer and the substrate. **e** A top view of the atomic model of IF bilayer on WSe_2 obtained through a DFT calculation. Gray and purple rhombus indicate the unit cell of WSe_2 and IF bilayer. **f** The ADF image of IF bilayer stacking on WSe_2 with the different rotation angles 0° and 30° . Inset is the corresponding FFT, where the diffraction spots of WSe_2 , the 0° , and 30° rotated IF layers are highlighted by white, cyan, and yellow hexagons. The scale bar is 2 nm. **g** The inverted FFT filtered image of the IF layer with the WSe_2 contrast been removed. The scale bar is 2 nm. **h** The simulated STEM-ADF image of the 30° rotated IF bilayer on WSe_2 . Inset is a raw ADF image of the 30° rotated IF region cropped from (**f**) for comparison. The scale bar is 1 nm.

edge of the furnace was at about 600°C . The growth time was 15 min. After the growth, the furnace was cooled down to room temperature with a cooling rate of 0.3°C s^{-1} .

Scanning transmission electron microscopy and electron energy loss spectroscopy

STEM images were acquired by using an ARM200F-based UHV microscope equipped with a JEOL delta corrector and a cold field emission gun operating at 60 kV. The probe current is about 15 pA. The convergence semi-angle and the inner acquisition semi-angle are 37 and 76 mrad. Typical ADF image was 1024×1024 pixels resolution captured by using $38.5 \mu\text{s}$ pixel time. The EELS core-loss spectra were taken by using Gatan Rio CMOS camera optimized for low-voltage operation. EEL spectrum was acquired by using a line scan with an exposure time of 0.1 s pixel^{-1} .

DFT calculation

We performed structure search using the evolutionary algorithm implemented in USPEX code^{24–26} combined with Vienna ab initio simulation package²⁷. Variable-composition 2D structure search was performed within the thickness of 0–4 Å and a total number of atoms 2–10. The initial population of IF structures was generated randomly under the 80-layer group symmetry. DFT calculations for structure searching and electronic property analyses were carried out within the projector-augmented wave method²⁸ and the exchange-correlation part was treated using the generalized gradient approximation of Perdew–Burke–Ernzerhof functional code²⁹. Van der Waals interaction was correlated using Grimme’s DFT-D3 method³⁰.

For the structural searching, the plane-wave basis set was contained up to 400 eV and the Brillouin zone was sampled using $2\pi \times 0.06 \text{ \AA}^{-1}$ resolution of Monkhorst–Pack mesh. Structural optimization was

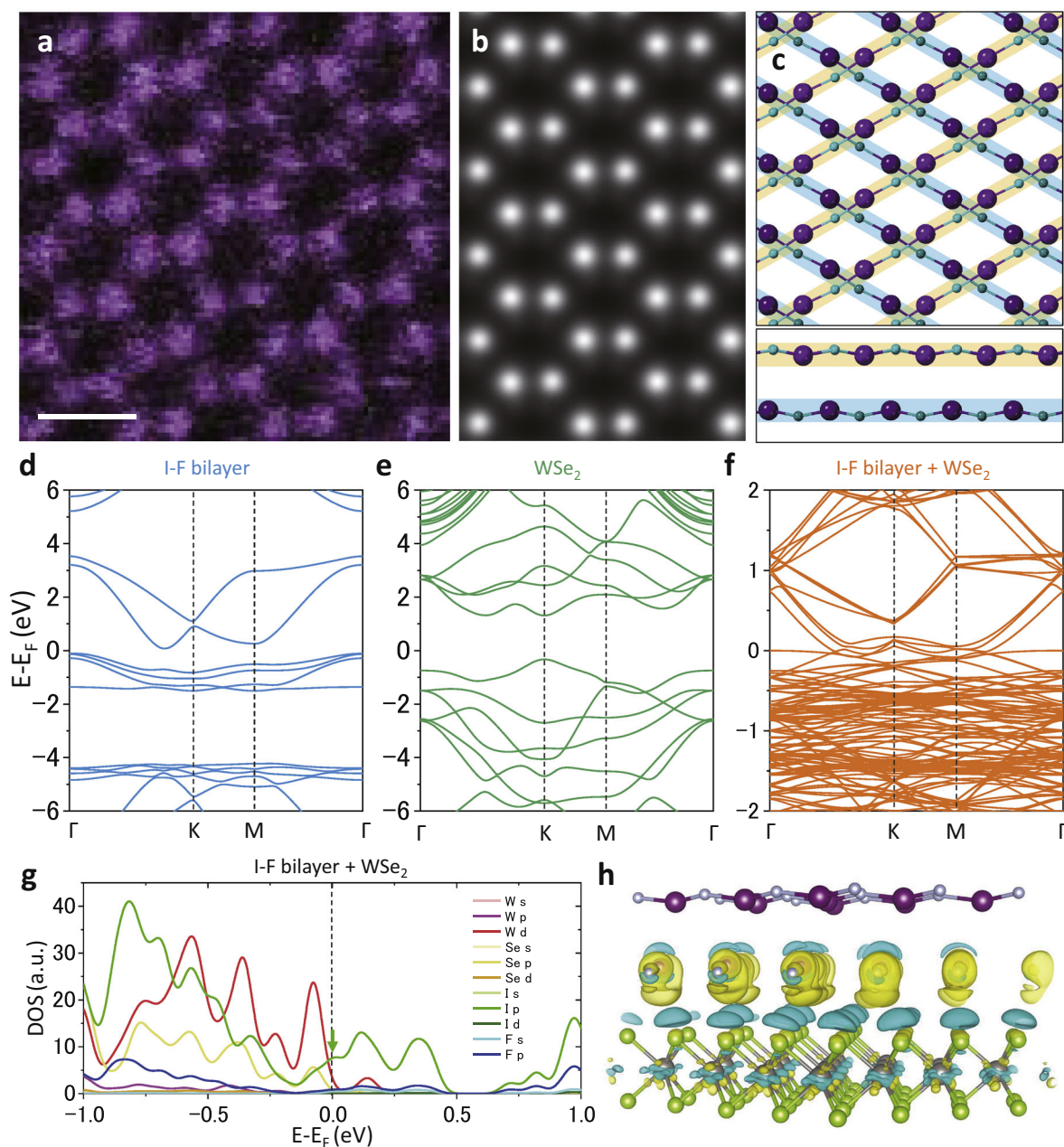


Fig. 4 **Theoretical electronic structure of the 2D IF layer on WSe_2 .** **a** A STEM-ADF image of the IF bilayer after the contrast due to the WSe_2 substrate has been removed. Bright atoms correspond to the iodine atoms ($Z = 53$). Fluorine atoms are hardly visible because of their smaller atomic number ($Z = 9$). The scale bar is 0.5 nm. **b** The STEM simulation image of the IF bilayer showing an excellent match with the experimentally derived atomic positions of iodine. **c** The corresponding atomic model of IF bilayer obtained through a DFT calculation. The top and bottom IF layers are colored by orange and blue ribbons, respectively. **d–f** DFT calculated band structures of free-standing IF bilayer, WSe_2 monolayer, and IF bilayer on WSe_2 substrate. Cusps at K in **(f)** are due to the asymmetric atomic positions of the IF bilayer. **g** Density of states analysis of IF bilayer on WSe_2 . Se p -states and I p -states (pointed by the green arrow) near the Fermi level contribute to the interaction between the IF bilayer and WSe_2 . The typical coupling between W d - and Se p -states of WSe_2 is also shown just below the Fermi level. **h** Charge difference analysis of IF bilayer on WSe_2 from separate IF bilayer and WSe_2 . Yellow and cyan colored regions indicate the charge accumulation and depletion, respectively. The isosurface was drawn at $5 \times 10^{-4} e \text{ \AA}^{-3}$.

performed until the Hellman–Feynman force of all atoms to be less than 0.02 eV \AA^{-1} .

For the electronic property analysis, the same basis set was used, and the Brillouin zone was sampled using $8 \times 8 \times 1$ Monkhorst–Pack meshes for the primitive unit cell of IF bilayer and WSe_2 monolayer. To simulate IF bilayer on WSe_2 substrate, 3×3 IF bilayer supercell was placed on 4×4 WSe_2 monolayer supercell, and $3 \times 3 \times 1$ Monkhorst–Pack mesh was used.

DATA AVAILABILITY

All data that support the findings of this study included in this published article and its Supplemental Material are available from the corresponding author upon request.

Received: 20 October 2020; Accepted: 7 January 2021;
Published online: 10 February 2021

REFERENCES

- Novoselov, K. S. et al. Electric field effect in atomically thin carbon films. *Science* **306**, 666–669 (2004).
- Tao, L. et al. Silicene field-effect transistors operating at room temperature. *Nat. Nanotechnol.* **10**, 227–231 (2015).
- Dávila, M. E., Xian, L., Cahangirov, S., Rubio, A. & Lay, G. L. E. Germanene: a novel two-dimensional germanium allotrope akin to graphene and silicene. *N. J. Phys.* **16**, 095002 (2014).
- Alducin, D., Myers, B. D., Liu, X. & Fisher, B. L. Synthesis of borophenes: anisotropic, two-dimensional boron polymorphs. *Science* **350**, 1513–1516 (2015).
- Li, L. et al. Black phosphorus field-effect transistors. *Nat. Nanotechnol.* **9**, 372–377 (2014).
- Dean, C. R. et al. Boron nitride substrates for high-quality graphene electronics. *Nat. Nanotechnol.* **5**, 722–726 (2010).
- Zhou, J. et al. A library of atomically thin metal chalcogenides. *Nature* **556**, 355–359 (2018).
- Li, G. et al. Epitaxial growth and physical properties of 2D materials beyond graphene: From monatomic materials to binary compounds. *Chem. Soc. Rev.* **47**, 6073–6100 (2018).
- Momeni, K. et al. Multiscale computational understanding and growth of 2D materials: a review. *npj Comput. Mater.* **6**, 22 (2020).
- Jones, R. G. Halogen adsorption on solid surfaces. *Prog. Surf. Sci.* **27**, 25–160 (1988).
- Frank, D. G., Chyan, O. M. R., Golden, T. & Hubbard, A. T. Probing three distinct iodine monolayer structures at Pt(111) by means of angular distribution Auger microscopy: results agree with scanning tunneling microscopy. *J. Phys. Chem.* **97**, 3829–3837 (1993).
- Felter, T. E. & Hubbard, A. T. L.e.e.d. and electrochemistry of iodine on Pt(100) and Pt(111) single-crystal surfaces. *J. Electroanal. Chem.* **100**, 473–491 (1979).
- Legma, J. B., Vacquier, G. & Casalot, A. Chemical vapour transport of molybdenum and tungsten diselenides by various transport agents. *J. Cryst. Growth* **130**, 253–258 (1993).
- Li, S. et al. Halide-assisted atmospheric pressure growth of large WSe₂ and WS₂ monolayer crystals. *Appl. Mater. Today* **1**, 60–66 (2015).
- Pisoni, A. et al. The role of transport agents in MoS₂ single crystals. *J. Phys. Chem. C* **119**, 3918–3922 (2015).
- Lin, Y. C. et al. Graphene annealing: how clean can it be? *Nano Lett.* **12**, 414–419 (2012).
- Lin, Y. C. et al. Clean transfer of graphene for isolation and suspension. *ACS Nano* **5**, 2362–2368 (2011).
- Durie, R. A. The electronic emission spectrum and molecular constants of iodine monofluoride. *Can. J. Phys.* **44**, 337–352 (1966).
- Harris, D. G., Blauer, J. A. & Hurlock, S. C. Iodine monofluoride discharge laser investigation. *J. Appl. Phys.* **68**, 3844–3848 (1990).
- De Young, R. J. Lasing characteristics of iodine monofluoride. *Appl. Phys. Lett.* **37**, 690–692 (1980).
- Hoyer, S. & Seppelt, K. The structure of IF₃. *Angew. Chem. Int. Ed.* **39**, 1448–1449 (2000).
- Zhang, L. et al. Crystal structure and properties of iodine monofluoride compounds at high pressure. *J. Phys. Condens. Matter* **32**, 385404 (2020).
- Luo, D. et al. A hypervalent and cubically coordinated molecular phase of IF₈ predicted at high pressure. *Chem. Sci.* **10**, 2543–2550 (2019).
- Oganov, A. R. & Glass, C. W. Crystal structure prediction using ab initio evolutionary techniques: principles and applications. *J. Chem. Phys.* **124**, 244704 (2006).
- Oganov, A. R., Lyakhov, A. O. & Valle, M. How evolutionary crystal structure prediction works-and why. *Acc. Chem. Res.* **44**, 227–237 (2011).
- Lyakhov, A. O., Oganov, A. R., Stokes, H. T. & Zhu, Q. New developments in evolutionary structure prediction algorithm USPEX. *Comput. Phys. Commun.* **184**, 1172–1182 (2013).
- Kresse, G. & Furthmüller, J. Efficient iterative schemes for ab initio total-energy calculations using a plane-wave basis set. *Phys. Rev. B* **54**, 11169–11186 (1996).
- Blöchl, P. E. Projector augmented-wave method. *Phys. Rev. B* **50**, 17953–17979 (1994).
- Perdew, J. P., Burke, K. & Ernzerhof, M. Generalized gradient approximation made simple. *Phys. Rev. Lett.* **77**, 3865–3868 (1996).
- Grimme, S. Semiempirical GGA-type density functional constructed with a long-range dispersion correction. *J. Comput. Chem.* **27**, 1787–1799 (2006).

ACKNOWLEDGEMENTS

Y.-C.L. and K.S. acknowledge to the JSPS-KAKENHI (JP16H06333), (18K14119), JST-CREST programs (JPMJCR20B1, JMJC20B5, and JPMJCR1993), JSPS A3 Foresight Program, and Kazato Research Encouragement Prize. G.-D.L. and S.L. acknowledge support from the National Research Foundation (NRF) of Korea grant (RIAM 2019R1A2C2005098, 2019R1A6A3A01091287, and 2017M3D1A1040688) and the Supercomputing Center/Korea Institute of Science and Technology Information with supercomputing resources (KSC-2018). P.-W.C. appreciates the project support of Taiwan Ministry of Science and Technology: Grants MOST 107-2119-M-007-011-MY2 and MOST 106-2628-M-007-003-MY3.

AUTHOR CONTRIBUTIONS

Y.-C.Y. and P.-W.C. contributed to the material synthesis. Y.-C.L. performed STEM-EELS experiment and data analysis. S.L. and G.-D.L. carried out the DFT calculation. Y.-C.L. and K.S. designed this work and wrote the paper. S.L., G.-D.L., and P.-W.C. discussed the experimental results and commented on the paper.

COMPETING INTERESTS

The authors declare no competing interests.

ADDITIONAL INFORMATION

Supplementary information The online version contains supplementary material available at <https://doi.org/10.1038/s41699-021-00201-8>.

Correspondence and requests for materials should be addressed to Y.-C.L., P.-W.C. or G.-D.L.

Reprints and permission information is available at <http://www.nature.com/reprints>

Publisher's note Springer Nature remains neutral with regard to jurisdictional claims in published maps and institutional affiliations.



Open Access This article is licensed under a Creative Commons Attribution 4.0 International License, which permits use, sharing, adaptation, distribution and reproduction in any medium or format, as long as you give appropriate credit to the original author(s) and the source, provide a link to the Creative Commons license, and indicate if changes were made. The images or other third party material in this article are included in the article's Creative Commons license, unless indicated otherwise in a credit line to the material. If material is not included in the article's Creative Commons license and your intended use is not permitted by statutory regulation or exceeds the permitted use, you will need to obtain permission directly from the copyright holder. To view a copy of this license, visit <http://creativecommons.org/licenses/by/4.0/>.

© The Author(s) 2021